

Search for $X(3872) \rightarrow \pi^0 \pi^0 \chi_{c1,2}$

M. Ablikim¹, M. N. Achasov^{4,c}, P. Adlarson⁷⁵, O. Afedulidis³, X. C. Ai⁸⁰, R. Aliberti³⁵, A. Amoroso^{74A,74C}, Q. An^{71,58,a}, Y. Bai⁵⁷, O. Bakina³⁶, I. Balossino^{29A}, Y. Ban^{46,h}, H.-R. Bao⁶³, V. Batzskaya^{1,44}, K. Begzsuren³², N. Berger³⁵, M. Berlowski⁴⁴, M. Bertani^{28A}, D. Bettoni^{29A}, F. Bianchi^{74A,74C}, E. Bianco^{74A,74C}, A. Bortone^{74A,74C}, I. Boyko³⁶, R. A. Briere⁵, A. Brueggemann⁶⁸, H. Cai⁷⁶, X. Cai^{1,58}, A. Calcaterra^{28A}, G. F. Cao^{1,63}, N. Cao^{1,63}, S. A. Cetin^{62A}, J. F. Chang^{1,58}, G. R. Che⁴³, G. Chelkov^{36,b}, C. Chen⁴³, C. H. Chen⁹, Chao Chen⁵⁵, G. Chen¹, H. S. Chen^{1,63}, H. Y. Chen²⁰, M. L. Chen^{1,58,63}, S. J. Chen⁴², S. L. Chen⁴⁵, S. M. Chen⁶¹, T. Chen^{1,63}, X. R. Chen^{31,63}, X. T. Chen^{1,63}, Y. B. Chen^{1,58}, Y. Q. Chen³⁴, Z. J. Chen^{25,i}, Z. Y. Chen^{1,63}, S. K. Choi^{10A}, G. Cibinetto^{29A}, F. Cossio^{74C}, J. J. Cui⁵⁰, H. L. Dai^{1,58}, J. P. Dai⁷⁸, A. Dbeyssi¹⁸, R. E. de Boer³, D. Dedovich³⁶, C. Q. Deng⁷², Z. Y. Deng¹, A. Denig³⁵, I. Denysenko³⁶, M. Destefanis^{74A,74C}, F. De Mori^{74A,74C}, B. Ding^{66,1}, X. X. Ding^{46,h}, Y. Ding⁴⁰, Y. Ding³⁴, J. Dong^{1,58}, L. Y. Dong^{1,63}, M. Y. Dong^{1,58,63}, X. Dong⁷⁶, M. C. Du¹, S. X. Du⁸⁰, Y. Y. Duan⁵⁵, Z. H. Duan⁴², P. Egorov^{36,b}, Y. H. Fan⁴⁵, J. Fang⁵⁹, J. Fang^{1,58}, S. S. Fang^{1,63}, W. X. Fang¹, Y. Fang¹, Y. Q. Fang^{1,58}, R. Farinelli^{29A}, L. Fava^{74B,74C}, F. Feldbauer³, G. Felici^{28A}, C. Q. Feng^{1,58}, J. H. Feng⁵⁹, Y. T. Feng^{71,58}, M. Fritsch³, C. D. Fu¹, J. L. Fu⁶³, Y. W. Fu^{1,63}, H. Gao⁶³, X. B. Gao⁴¹, Y. N. Gao^{46,h}, Yang Gao^{71,58}, S. Garbolino^{74C}, I. Garzia^{29A,29B}, L. Ge⁸⁰, P. T. Ge⁷⁶, Z. W. Ge⁴², C. Geng⁵⁹, E. M. Gersabeck⁶⁷, A. Gilman⁶⁹, K. Goetzen¹³, L. Gong⁴⁰, W. X. Gong^{1,58}, W. Gradl³⁵, S. Gramigna^{29A,29B}, M. Greco^{74A,74C}, M. H. Gu^{1,58}, Y. T. Gu¹⁵, C. Y. Guan^{1,63}, A. Q. Guo^{31,63}, L. B. Guo⁴¹, M. J. Guo⁵⁰, R. P. Guo⁴⁹, Y. P. Guo^{12,g}, A. Guskov^{36,b}, J. Gutierrez²⁷, K. L. Han⁶³, T. T. Han¹, F. Hanisch³, X. Q. Hao¹⁹, F. A. Harris⁶⁵, K. K. He⁵⁵, K. L. He^{1,63}, F. H. Heinsius³, C. H. Heinz³⁵, Y. K. Heng^{1,58,63}, C. Herold⁶⁰, T. Holtmann³, P. C. Hong³⁴, G. Y. Hou^{1,63}, X. T. Hou^{1,63}, Y. R. Hou⁶³, Z. L. Hou¹, B. Y. Hu⁵⁹, H. M. Hu^{1,63}, J. F. Hu^{56,j}, S. L. Hu^{12,g}, T. Hu^{1,58,63}, Y. Hu¹, G. S. Huang^{71,58}, K. X. Huang⁵⁹, L. Q. Huang^{31,63}, X. T. Huang⁵⁰, Y. P. Huang¹, Y. S. Huang⁵⁹, T. Hussain⁷³, F. Hölzken³, N. Hüskens³⁵, N. in der Wiesche⁶⁸, J. Jackson²⁷, S. Janchiv³², J. H. Jeong^{10A}, Q. Ji¹, Q. P. Ji¹⁹, W. Ji^{1,63}, X. B. Ji^{1,63}, X. L. Ji^{1,58}, Y. Y. Ji⁵⁰, X. Q. Jia⁵⁰, Z. K. Jia^{71,58}, D. Jiang^{1,63}, H. B. Jiang⁷⁶, P. C. Jiang^{46,h}, S. S. Jiang³⁹, T. J. Jiang¹⁶, X. S. Jiang^{1,58,63}, Y. Jiang⁶³, J. B. Jiao⁵⁰, J. K. Jiao³⁴, Z. Jiao²³, S. Jin⁴², Y. Jin⁶⁶, M. Q. Jing^{1,63}, X. M. Jing⁶³, T. Johansson⁷⁵, S. Kabana³³, N. Kalantar-Nayestanaki⁶⁴, X. L. Kang⁹, X. S. Kang⁴⁰, M. Kavatsyuk⁶⁴, B. C. Ke⁸⁰, V. Khachatryan²⁷, A. Khoukaz⁶⁸, R. Kiuchi¹, O. B. Kolcu^{62A}, B. Kopf³, M. Kuessner³, X. Kui^{1,63}, N. Kumar²⁶, A. Kupsc^{44,75}, W. Kühn³⁷, J. J. Lane⁶⁷, P. Larin¹⁸, L. Lavezzi^{74A,74C}, T. T. Lei^{71,58}, Z. H. Lei^{71,58}, M. Lellmann³⁵, T. Lenz³⁵, C. Li⁴³, C. Li⁴⁷, C. H. Li³⁹, Cheng Li^{71,58}, D. M. Li⁸⁰, F. Li^{1,58}, G. Li¹, H. B. Li^{1,63}, H. J. Li¹⁹, H. N. Li^{56,j}, Hui Li⁴³, J. R. Li⁶¹, J. S. Li⁵⁹, K. Li¹, L. J. Li^{1,63}, L. K. Li¹, Lei Li⁴⁸, M. H. Li⁴³, P. R. Li^{38,k,l}, Q. M. Li^{1,63}, Q. X. Li⁵⁰, R. Li^{17,31}, S. X. Li¹², T. Li⁵⁰, W. D. Li^{1,63}, W. G. Li^{1,a}, X. Li^{1,63}, X. H. Li^{71,58}, X. L. Li⁵⁰, X. Y. Li^{1,63}, X. Z. Li⁵⁹, Y. G. Li^{46,h}, Z. Y. Li⁵⁹, Z. Y. Li⁷⁸, C. Liang⁴², H. Liang^{1,63}, H. Liang^{71,58}, Y. F. Liang⁵⁴, Y. T. Liang^{31,63}, G. R. Liao¹⁴, L. X. Liao⁵⁰, Y. P. Liao^{1,63}, J. Libby²⁶, A. Limphirat⁶⁰, C. C. Lin⁵⁵, D. X. Lin^{31,63}, T. Lin¹, B. J. Liu¹, B. X. Liu⁷⁶, C. Liu³⁴, C. X. Liu¹, F. Liu¹, F. H. Liu⁵³, Feng Liu⁶, G. M. Liu^{56,j}, H. Liu^{38,k,l}, H. B. Liu¹⁵, H. H. Liu¹, H. M. Liu^{1,63}, Huihui Liu²¹, J. B. Liu^{71,58}, J. Y. Liu^{1,63}, K. Liu^{38,k,l}, K. Y. Liu⁴⁰, Ke Liu²², L. Liu^{71,58}, L. C. Liu⁴³, Lu Liu⁴³, M. H. Liu^{12,g}, P. L. Liu¹, Q. Liu⁶³, S. B. Liu^{71,58}, T. Liu^{12,g}, W. K. Liu⁴³, W. M. Liu^{71,58}, X. Liu^{38,k,l}, X. Liu³⁹, Y. Liu⁸⁰, Y. Liu^{38,k,l}, Y. B. Liu⁴³, Z. A. Liu^{1,58,63}, Z. D. Liu⁹, Z. Q. Liu⁵⁰, X. C. Lou^{1,58,63}, F. X. Lu⁵⁹, H. J. Lu²³, J. G. Lu^{1,58}, X. L. Lu¹, Y. Lu⁷, Y. P. Lu^{1,58}, Z. H. Lu^{1,63}, C. L. Luo⁴¹, J. R. Luo⁵⁹, M. X. Luo⁷⁹, T. Luo^{12,g}, X. L. Luo^{1,58}, X. R. Lyu⁶³, Y. F. Lyu⁴³, F. C. Ma⁴⁰, H. Ma⁷⁸, H. L. Ma¹, J. L. Ma^{1,63}, L. L. Ma⁵⁰, M. M. Ma^{1,63}, Q. M. Ma¹, R. Q. Ma^{1,63}, T. Ma^{71,58}, X. T. Ma^{1,63}, X. Y. Ma^{1,58}, Y. Ma^{46,h}, Y. M. Ma³¹, F. E. Maas¹⁸, M. Maggiora^{74A,74C}, S. Malde⁶⁹, Y. J. Mao^{46,h}, Z. P. Mao¹, S. Marcello^{74A,74C}, Z. X. Meng⁶⁶, J. G. Messchendorp^{13,64}, G. Mezzadri^{29A}, H. Miao^{1,63}, T. J. Min⁴², R. E. Mitchell²⁷, X. H. Mo^{1,58,63}, B. Moses²⁷, N. Yu. Muchnoi^{4,c}, J. Muskalla³⁵, Y. Nefedov³⁶, F. Nerling^{18,e}, L. S. Nie²⁰, I. B. Nikolaev^{4,c}, Z. Ning^{1,58}, S. Nisar^{11,m}, Q. L. Niu^{38,k,l}, W. D. Niu⁵⁵, Y. Niu⁵⁰, S. L. Olsen⁶³, Q. Ouyang^{1,58,63}, S. Pacetti^{28B,28C}, X. Pan⁵⁵, Y. Pan⁵⁷, A. Pathak³⁴, P. Patteri^{28A}, Y. P. Pei^{71,58}, M. Pelizaeus³, H. P. Peng^{71,58}, Y. Y. Peng^{38,k,l}, K. Peters^{13,e}, J. L. Ping⁴¹, R. G. Ping^{1,63}, S. Plura³⁵, V. Prasad³³, F. Z. Qi¹, H. Qi^{71,58}, H. R. Qi⁶¹, M. Qi⁴², T. Y. Qi^{12,g}, S. Qian^{1,58}, W. B. Qian⁶³, C. F. Qiao⁶³, X. K. Qiao⁸⁰, J. J. Qin⁷², L. Q. Qin¹⁴, L. Y. Qin^{71,58}, X. S. Qin⁵⁰, Z. H. Qin^{1,58}, J. F. Qiu¹, Z. H. Qu⁷², C. F. Redmer³⁵, K. J. Ren³⁹, A. Rivetti^{74C}, M. Rolo^{74C}, G. Rong^{1,63}, Ch. Rosner¹⁸, S. N. Ruan⁴³, N. Salone⁴⁴, A. Sarantsev^{36,d}, Y. Schelhaas³⁵, K. Schoenning⁷⁵, M. Scodreggio^{29A}, K. Y. Shan^{12,g}, W. Shan²⁴, X. Y. Shan^{71,58}, Z. J. Shang^{38,k,l}, J. F. Shangguan¹⁶, L. G. Shao^{1,63}, M. Shao^{71,58}, C. P. Shen^{12,g}, H. F. Shen^{1,8}, W. H. Shen⁶³, X. Y. Shen^{1,63}, B. A. Shi⁶³, H. Shi^{71,58}, H. C. Shi^{71,58}, J. L. Shi^{12,g}, J. Y. Shi¹, Q. Q. Shi⁵⁵, S. Y. Shi⁷², X. Shi^{1,58}, J. J. Song¹⁹, T. Z. Song⁵⁹, W. M. Song^{34,1}, Y. J. Song^{12,g}, Y. X. Song^{46,h,n}, S. Sosio^{74A,74C}, S. Spataro^{74A,74C}, F. Stieler³⁵, Y. J. Su⁶³, G. B. Sun⁷⁶, G. X. Sun¹, H. Sun⁶³, H. K. Sun¹, J. F. Sun¹⁹, K. Sun⁶¹, L. Sun⁷⁶, S. S. Sun^{1,63}, T. Sun^{51,f}, W. Y. Sun³⁴, Y. Sun⁹, Y. J. Sun^{71,58}, Y. Z. Sun¹, Z. Q. Sun^{1,63}, Z. T. Sun⁵⁰, C. J. Tang⁵⁴, G. Y. Tang¹, J. Tang⁵⁹, M. Tang^{71,58}, Y. A. Tang⁷⁶, L. Y. Tao⁷², Q. T. Tao^{25,i}, M. Tat⁶⁹, J. X. Teng^{71,58}, V. Thoren⁵⁵, W. H. Tian⁵⁹, Y. Tian^{31,63}, Z. F. Tian⁷⁶, I. Uman^{62B}, Y. Wan⁵⁵, S. J. Wang⁵⁰, B. Wang¹, B. L. Wang⁶³, Bo Wang^{71,58}, D. Y. Wang^{46,h}, F. Wang⁷², H. J. Wang^{38,k,l}, J. J. Wang⁷⁶, J. P. Wang⁵⁰, K. Wang^{1,58}, L. L. Wang¹, M. Wang⁵⁰, N. Y. Wang⁶³, S. Wang^{12,g}, S. Wang^{38,k,l}, T. Wang^{12,g}, T. J. Wang⁴³, W. Wang⁷², W. Wang⁵⁹, W. P. Wang^{35,71,o}, X. Wang^{46,h}, X. F. Wang^{38,k,l}, X. J. Wang³⁹, X. L. Wang^{12,g}, X. N. Wang¹, Y. Wang⁶¹, Y. D. Wang⁴⁵, Y. F. Wang^{1,58,63}, Y. L. Wang¹⁹, Y. N. Wang⁴⁵, Y. Q. Wang¹, Yaqian Wang¹⁷, Yi Wang⁶¹, Z. Wang^{1,58}, Z. L. Wang⁷², Z. Y. Wang^{1,63}, Ziyi Wang⁶³, D. H. Wei¹⁴, F. Weidner⁶⁸, S. P. Wen¹, Y. R. Wen³⁹, U. Wiedner³, G. Wilkinson⁶⁹, M. Wolke⁷⁵, L. Wollenberg³, C. Wu³⁹, J. F. Wu^{1,8}, L. H. Wu¹, L. J. Wu^{1,63}, X. Wu^{12,g}, X. H. Wu³⁴, Y. Wu^{71,58}, Y. H. Wu⁵⁵, Y. J. Wu³¹, Z. Wu^{1,58}, L. Xia^{71,58}, X. M. Xian³⁹, B. H. Xiang^{1,63}, T. Xiang^{46,h}, D. Xiao^{38,k,l}, G. Y. Xiao⁴², S. Y. Xiao¹, Y. L. Xiao^{12,g}, Z. J. Xiao⁴¹, C. Xie⁴², X. H. Xie^{46,h}, Y. Xie⁵⁰, Y. G. Xie^{1,58}, Y. H. Xie⁶, Z. P. Xie^{71,58}, T. Y. Xing^{1,63}, C. F. Xu^{1,63}, C. J. Xu⁵⁹, G. F. Xu¹, H. Y. Xu^{66,2,p}, M. Xu^{71,58}, Q. J. Xu¹⁶, Q. N. Xu³⁰, W. Xu¹, W. L. Xu⁶⁶, X. P. Xu⁵⁵, Y. C. Xu⁷⁷, Z. P. Xu⁴², Z. S. Xu⁶³, F. Yan^{12,g}

L. Yan^{12,g}, W. B. Yan^{71,58}, W. C. Yan⁸⁰, X. Q. Yan¹, H. J. Yang^{51,f}, H. L. Yang³⁴, H. X. Yang¹, T. Yang¹, Y. Yang^{12,g},
 Y. F. Yang⁴³, Y. F. Yang^{1,63}, Y. X. Yang^{1,63}, Z. W. Yang^{38,k,l}, Z. P. Yao⁵⁰, M. Ye^{1,58}, M. H. Ye⁸, J. H. Yin¹, Z. Y. You⁵⁹,
 B. X. Yu^{1,58,63}, C. X. Yu⁴³, G. Yu^{1,63}, J. S. Yu^{25,i}, T. Yu⁷², X. D. Yu^{46,h}, Y. C. Yu⁸⁰, C. Z. Yuan^{1,63}, J. Yuan⁴⁵, J. Yuan³⁴,
 L. Yuan², S. C. Yuan^{1,63}, Y. Yuan^{1,63}, Z. Y. Yuan⁵⁹, C. X. Yue³⁹, A. A. Zafar⁷³, F. R. Zeng⁵⁰, S. H. Zeng⁷², X. Zeng^{12,g},
 Y. Zeng^{25,i}, Y. J. Zeng^{1,63}, Y. J. Zeng⁵⁹, X. Y. Zhai³⁴, Y. C. Zhai⁵⁰, Y. H. Zhan⁵⁹, A. Q. Zhang^{1,63}, B. L. Zhang^{1,63},
 B. X. Zhang¹, D. H. Zhang⁴³, G. Y. Zhang¹⁹, H. Zhang⁸⁰, H. Zhang^{71,58}, H. C. Zhang^{1,58,63}, H. H. Zhang⁵⁹, H. H. Zhang³⁴,
 H. Q. Zhang^{1,58,63}, H. R. Zhang^{71,58}, H. Y. Zhang^{1,58}, J. Zhang⁸⁰, J. Zhang⁵⁹, J. J. Zhang⁵², J. L. Zhang²⁰, J. Q. Zhang⁴¹,
 J. S. Zhang^{12,g}, J. W. Zhang^{1,58,63}, J. X. Zhang^{38,k,l}, J. Y. Zhang¹, J. Z. Zhang^{1,63}, Jianyu Zhang⁶³, L. M. Zhang⁶¹,
 Lei Zhang⁴², P. Zhang^{1,63}, Q. Y. Zhang³⁴, R. Y. Zhang^{38,k,l}, S. H. Zhang^{1,63}, Shulei Zhang^{25,i}, X. D. Zhang⁴⁵, X. M. Zhang¹,
 X. Y. Zhang⁵⁰, Y. Zhang⁷², Y. Zhang¹, Y. T. Zhang⁸⁰, Y. H. Zhang^{1,58}, Y. M. Zhang³⁹, Yan Zhang^{71,58}, Z. D. Zhang¹,
 Z. H. Zhang¹, Z. L. Zhang³⁴, Z. Y. Zhang⁴³, Z. Y. Zhang⁷⁶, Z. Z. Zhang⁴⁵, G. Zhao¹, J. Y. Zhao^{1,63}, J. Z. Zhao^{1,58},
 L. Zhao¹, Lei Zhao^{71,58}, M. G. Zhao⁴³, N. Zhao⁷⁸, R. P. Zhao⁶³, S. J. Zhao⁸⁰, Y. B. Zhao^{1,58}, Y. X. Zhao^{31,63},
 Z. G. Zhao^{71,58}, A. Zhemchugov^{36,b}, B. Zheng⁷², B. M. Zheng³⁴, J. P. Zheng^{1,58}, W. J. Zheng^{1,63}, Y. H. Zheng⁶³, B. Zhong⁴¹,
 X. Zhong⁵⁹, H. Zhou⁵⁰, J. Y. Zhou³⁴, L. P. Zhou^{1,63}, S. Zhou⁶, X. Zhou⁷⁶, X. K. Zhou⁶, X. R. Zhou^{71,58}, X. Y. Zhou³⁹,
 Y. Z. Zhou^{12,g}, J. Zhu⁴³, K. Zhu¹, K. J. Zhu^{1,58,63}, K. S. Zhu^{12,g}, L. Zhu³⁴, L. X. Zhu⁶³, S. H. Zhu⁷⁰, S. Q. Zhu⁴²,
 T. J. Zhu^{12,g}, W. D. Zhu⁴¹, Y. C. Zhu^{71,58}, Z. A. Zhu^{1,63}, J. H. Zou¹, J. Zu^{71,58}

(BESIII Collaboration)

¹ Institute of High Energy Physics, Beijing 100049, People's Republic of China

² Beihang University, Beijing 100191, People's Republic of China

³ Bochum Ruhr-University, D-44780 Bochum, Germany

⁴ Budker Institute of Nuclear Physics SB RAS (BINP), Novosibirsk 630090, Russia

⁵ Carnegie Mellon University, Pittsburgh, Pennsylvania 15213, USA

⁶ Central China Normal University, Wuhan 430079, People's Republic of China

⁷ Central South University, Changsha 410083, People's Republic of China

⁸ China Center of Advanced Science and Technology, Beijing 100190, People's Republic of China

⁹ China University of Geosciences, Wuhan 430074, People's Republic of China

¹⁰ Chung-Ang University, Seoul, 06974, Republic of Korea

¹¹ COMSATS University Islamabad, Lahore Campus, Defence Road, Off Raiwind Road, 54000 Lahore, Pakistan

¹² Fudan University, Shanghai 200433, People's Republic of China

¹³ GSI Helmholtzcentre for Heavy Ion Research GmbH, D-64291 Darmstadt, Germany

¹⁴ Guangxi Normal University, Guilin 541004, People's Republic of China

¹⁵ Guangxi University, Nanning 530004, People's Republic of China

¹⁶ Hangzhou Normal University, Hangzhou 310036, People's Republic of China

¹⁷ Hebei University, Baoding 071002, People's Republic of China

¹⁸ Helmholtz Institute Mainz, Staudinger Weg 18, D-55099 Mainz, Germany

¹⁹ Henan Normal University, Xinxiang 453007, People's Republic of China

²⁰ Henan University, Kaifeng 475004, People's Republic of China

²¹ Henan University of Science and Technology, Luoyang 471003, People's Republic of China

²² Henan University of Technology, Zhengzhou 450001, People's Republic of China

²³ Huangshan College, Huangshan 245000, People's Republic of China

²⁴ Hunan Normal University, Changsha 410081, People's Republic of China

²⁵ Hunan University, Changsha 410082, People's Republic of China

²⁶ Indian Institute of Technology Madras, Chennai 600036, India

²⁷ Indiana University, Bloomington, Indiana 47405, USA

²⁸ INFN Laboratori Nazionali di Frascati, (A)INFN Laboratori Nazionali di Frascati, I-00044, Frascati, Italy; (B)INFN

Sezione di Perugia, I-06100, Perugia, Italy; (C)University of Perugia, I-06100, Perugia, Italy

²⁹ INFN Sezione di Ferrara, (A)INFN Sezione di Ferrara, I-44122, Ferrara, Italy; (B)University of Ferrara, I-44122, Ferrara, Italy

³⁰ Inner Mongolia University, Hohhot 010021, People's Republic of China

³¹ Institute of Modern Physics, Lanzhou 730000, People's Republic of China

³² Institute of Physics and Technology, Peace Avenue 54B, Ulaanbaatar 13330, Mongolia

³³ Instituto de Alta Investigación, Universidad de Tarapacá, Casilla 7D, Arica 1000000, Chile

³⁴ Jilin University, Changchun 130012, People's Republic of China

³⁵ Johannes Gutenberg University of Mainz, Johann-Joachim-Becher-Weg 45, D-55099 Mainz, Germany

³⁶ Joint Institute for Nuclear Research, 141980 Dubna, Moscow region, Russia

³⁷ Justus-Liebig-Universität Giessen, II. Physikalisches Institut, Heinrich-Buff-Ring 16, D-35392 Giessen, Germany

³⁸ Lanzhou University, Lanzhou 730000, People's Republic of China

³⁹ Liaoning Normal University, Dalian 116029, People's Republic of China

⁴⁰ Liaoning University, Shenyang 110036, People's Republic of China

⁴¹ Nanjing Normal University, Nanjing 210023, People's Republic of China

⁴² Nanjing University, Nanjing 210093, People's Republic of China

⁴³ Nankai University, Tianjin 300071, People's Republic of China

- ⁴⁴ National Centre for Nuclear Research, Warsaw 02-093, Poland
- ⁴⁵ North China Electric Power University, Beijing 102206, People's Republic of China
- ⁴⁶ Peking University, Beijing 100871, People's Republic of China
- ⁴⁷ Qufu Normal University, Qufu 273165, People's Republic of China
- ⁴⁸ Renmin University of China, Beijing 100872, People's Republic of China
- ⁴⁹ Shandong Normal University, Jinan 250014, People's Republic of China
- ⁵⁰ Shandong University, Jinan 250100, People's Republic of China
- ⁵¹ Shanghai Jiao Tong University, Shanghai 200240, People's Republic of China
- ⁵² Shanxi Normal University, Linfen 041004, People's Republic of China
- ⁵³ Shanxi University, Taiyuan 030006, People's Republic of China
- ⁵⁴ Sichuan University, Chengdu 610064, People's Republic of China
- ⁵⁵ Soochow University, Suzhou 215006, People's Republic of China
- ⁵⁶ South China Normal University, Guangzhou 510006, People's Republic of China
- ⁵⁷ Southeast University, Nanjing 211100, People's Republic of China
- ⁵⁸ State Key Laboratory of Particle Detection and Electronics, Beijing 100049, Hefei 230026, People's Republic of China
- ⁵⁹ Sun Yat-Sen University, Guangzhou 510275, People's Republic of China
- ⁶⁰ Suranaree University of Technology, University Avenue 111, Nakhon Ratchasima 30000, Thailand
- ⁶¹ Tsinghua University, Beijing 100084, People's Republic of China
- ⁶² Turkish Accelerator Center Particle Factory Group, (A)Istinye University, 34010, Istanbul, Turkey; (B)Near East University, Nicosia, North Cyprus, 99138, Mersin 10, Turkey
- ⁶³ University of Chinese Academy of Sciences, Beijing 100049, People's Republic of China
- ⁶⁴ University of Groningen, NL-9747 AA Groningen, The Netherlands
- ⁶⁵ University of Hawaii, Honolulu, Hawaii 96822, USA
- ⁶⁶ University of Jinan, Jinan 250022, People's Republic of China
- ⁶⁷ University of Manchester, Oxford Road, Manchester, M13 9PL, United Kingdom
- ⁶⁸ University of Muenster, Wilhelm-Klemm-Strasse 9, 48149 Muenster, Germany
- ⁶⁹ University of Oxford, Keble Road, Oxford OX13RH, United Kingdom
- ⁷⁰ University of Science and Technology Liaoning, Anshan 114051, People's Republic of China
- ⁷¹ University of Science and Technology of China, Hefei 230026, People's Republic of China
- ⁷² University of South China, Hengyang 421001, People's Republic of China
- ⁷³ University of the Punjab, Lahore-54590, Pakistan
- ⁷⁴ University of Turin and INFN, (A)University of Turin, I-10125, Turin, Italy; (B)University of Eastern Piedmont, I-15121, Alessandria, Italy; (C)INFN, I-10125, Turin, Italy
- ⁷⁵ Uppsala University, Box 516, SE-75120 Uppsala, Sweden
- ⁷⁶ Wuhan University, Wuhan 430072, People's Republic of China
- ⁷⁷ Yantai University, Yantai 264005, People's Republic of China
- ⁷⁸ Yunnan University, Kunming 650500, People's Republic of China
- ⁷⁹ Zhejiang University, Hangzhou 310027, People's Republic of China
- ⁸⁰ Zhengzhou University, Zhengzhou 450001, People's Republic of China
- ^a Deceased
- ^b Also at the Moscow Institute of Physics and Technology, Moscow 141700, Russia
- ^c Also at the Novosibirsk State University, Novosibirsk, 630090, Russia
- ^d Also at the NRC "Kurchatov Institute", PNPI, 188300, Gatchina, Russia
- ^e Also at Goethe University Frankfurt, 60323 Frankfurt am Main, Germany
- ^f Also at Key Laboratory for Particle Physics, Astrophysics and Cosmology, Ministry of Education; Shanghai Key Laboratory for Particle Physics and Cosmology; Institute of Nuclear and Particle Physics, Shanghai 200240, People's Republic of China
- ^g Also at Key Laboratory of Nuclear Physics and Ion-beam Application (MOE) and Institute of Modern Physics, Fudan University, Shanghai 200443, People's Republic of China
- ^h Also at State Key Laboratory of Nuclear Physics and Technology, Peking University, Beijing 100871, People's Republic of China
- ⁱ Also at School of Physics and Electronics, Hunan University, Changsha 410082, China
- ^j Also at Guangdong Provincial Key Laboratory of Nuclear Science, Institute of Quantum Matter, South China Normal University, Guangzhou 510006, China
- ^k Also at MOE Frontiers Science Center for Rare Isotopes, Lanzhou University, Lanzhou 730000, People's Republic of China
- ^l Also at Lanzhou Center for Theoretical Physics, Lanzhou University, Lanzhou 730000, People's Republic of China
- ^m Also at the Department of Mathematical Sciences, IBA, Karachi 75270, Pakistan
- ⁿ Also at Ecole Polytechnique Federale de Lausanne (EPFL), CH-1015 Lausanne, Switzerland
- ^o Also at Helmholtz Institute Mainz, Staudinger Weg 18, D-55099 Mainz, Germany
- ^p Also at School of Physics, Beihang University, Beijing 100191, China

(Dated: August 2, 2024)

Using 10.1 fb^{-1} of e^+e^- collision data collected by the BESIII detector with center-of-mass energies between 4.15 GeV and 4.30 GeV, we search for the decays $X(3872) \rightarrow$

$\pi^0\pi^0\chi_{c1,2}$, where the $X(3872)$ is produced in $e^+e^- \rightarrow \gamma X(3872)$. No evidence above 3σ is found for either decay. Upper limits at the 90% C.L. on the branching fractions of $X(3872) \rightarrow \pi^0\pi^0\chi_{c1,2}$ normalized to the branching fraction of $X(3872) \rightarrow \pi^+\pi^-J/\psi$ are set to be $\mathcal{B}(X(3872) \rightarrow \pi^0\pi^0\chi_{c1})/\mathcal{B}(X(3872) \rightarrow \pi^+\pi^-J/\psi) < 1.1$ and $\mathcal{B}(X(3872) \rightarrow \pi^0\pi^0\chi_{c2})/\mathcal{B}(X(3872) \rightarrow \pi^+\pi^-J/\psi) < 0.5$, taking into account both statistical and systematic uncertainties.

PACS numbers: 13.25.Gv, 12.38.Qk, 14.20.Gk, 14.40.Cs

I. INTRODUCTION

In 2003, the Belle Collaboration reported the first observation of the state $X(3872)$, also referred to as $\chi_{c1}(3872)$, in the decay $B^\pm \rightarrow X(3872)K^\pm$ [1]. This marked the beginning of the discovery of many charmonium-like states that exhibit clear discrepancies with a conventional charmonium ($c\bar{c}$) interpretation. While the $X(3872)$ has quantum numbers $J^{PC} = 1^{++}$ allowed by the $c\bar{c}$ model, its mass differs from the nearest expected $c\bar{c}$ state, the $\chi_{c1}(2P)$, by $100 \text{ MeV}/c^2$ [2]. The particularly narrow width of the $X(3872)$ of $(1.19 \pm 0.21) \text{ MeV}$ makes this difference especially stark [3, 4]. In addition, the $X(3872)$ is known to decay through many isospin violating channels, including $\rho^0 J/\psi$ [1] and $\pi^0\chi_{c1}$ [5].

Nearly two decades since its discovery, the $X(3872)$ lacks a definitive interpretation although several models have been proposed in order to explain its unusual properties. Due to its close proximity to the $D^0\bar{D}^{*0}$ threshold, the molecular $D^0\bar{D}^{*0} + \bar{D}^0D^{*0}$ interpretation offers a compelling possibility [6]. Two other explanations include a compact tetraquark interpretation [7] or a superposition between a molecular and a conventional charmonium state [8]. It is predicted that the branching fractions of the decays of the $X(3872)$ to $\pi\chi_{cJ}$ or $\pi\pi\chi_{cJ}$ ($J = 0, 1, 2$) depend on the internal structure of the $X(3872)$ [9, 10]. These pionic transitions of the $X(3872)$ to χ_{cJ} therefore serve as an excellent way to probe the quark configuration of the $X(3872)$.

A previous BESIII analysis [5] measured the single pion branching fraction ratio

$$\frac{\mathcal{B}(X(3872) \rightarrow \pi^0\chi_{c1})}{\mathcal{B}(X(3872) \rightarrow \pi^+\pi^-J/\psi)} = 0.88^{+0.33}_{-0.27} \pm 0.10,$$

where the first uncertainty is statistical and the second systematic, and placed upper limits of

$$\frac{\mathcal{B}(X(3872) \rightarrow \pi^0\chi_{c0})}{\mathcal{B}(X(3872) \rightarrow \pi^+\pi^-J/\psi)} < 19$$

and

$$\frac{\mathcal{B}(X(3872) \rightarrow \pi^0\chi_{c2})}{\mathcal{B}(X(3872) \rightarrow \pi^+\pi^-J/\psi)} < 1.1$$

at the 90% confidence level. Though these upper limits were consistent with both a conventional interpretation and a four-quark state (i.e. either a compact

tetraquark or a hadronic molecule), the measurement on $X(3872) \rightarrow \pi^0\pi^0\chi_{c1}$ was consistent with the four-quark state and disfavored the conventional picture. Another BESIII analysis [11] reduced the upper limit on the $J = 0$ decay to

$$\frac{\mathcal{B}(X(3872) \rightarrow \pi^0\chi_{c0})}{\mathcal{B}(X(3872) \rightarrow \pi^+\pi^-J/\psi)} < 3.6$$

at the 90% confidence level and placed upper limits on the two-pion decays to χ_{cJ} . However, none of the aforementioned upper limits are stringent enough to rule out additional interpretations for the $X(3872)$.

In this paper, we strengthen these results by searching for the decays $X(3872) \rightarrow \pi^0\pi^0\chi_{c1,2}$ with BESIII data. For $J = 1$, this decay is predicted to be extremely sensitive to the quark configuration of the $X(3872)$. For a conventional charmonium state, the ratio $\mathcal{B}(X(3872) \rightarrow \pi^0\pi^0\chi_{c1})/\mathcal{B}(X(3872) \rightarrow \pi^+\pi^-J/\psi)$ is expected to be approximately 12.5 [9]. Meanwhile, for a four-quark state, the same ratio is predicted to be approximately 0.61 [10]. This stark difference indicates that even an upper limit could provide key information disfavoring a conventional interpretation. Additionally, it is predicted that for $J = 2$, this ratio is further suppressed and on the order of 10^{-6} [10] for a molecular state.

We exclusively reconstruct the processes $X(3872) \rightarrow \pi^0\pi^0\chi_{c1,2}$, collectively called the search channel. The $X(3872)$ is produced alongside a photon, referred to as γ_1 throughout this paper, in e^+e^- collisions. The χ_{c1} and χ_{c2} are reconstructed via $\chi_{c1,2} \rightarrow \gamma_2 J/\psi$ and the J/ψ is reconstructed via $J/\psi \rightarrow e^+e^-$ or $J/\psi \rightarrow \mu^+\mu^-$. We refer to the photon produced alongside the J/ψ in $\chi_{c1,2}$ decays as γ_2 . The final state in the search channel is therefore $\gamma_1\gamma_2\pi^0\pi^0l^+l^-$, where each π^0 is reconstructed from two photons and l^+l^- refers to either an electron or muon pair.

With the same production of $X(3872)$ in the decay $e^+e^- \rightarrow \gamma X(3872)$, the branching fraction of the search channel is normalized to that of $X(3872) \rightarrow \pi^+\pi^-J/\psi$, referred to as the normalization channel throughout this paper. This cancels common systematic uncertainties.

II. DETECTOR AND DATA SAMPLES

The BESIII detector [12] records symmetric e^+e^- collisions provided by the BEPCII storage ring [13], which operates with a peak luminosity of $1 \times 10^{33} \text{ cm}^{-2}\text{s}^{-1}$ in the center-of-mass (CM) energy range from 2.0 to 4.95 GeV. BESIII has collected large data samples in this energy region [14]. The cylindrical core of the BESIII detector covers 93% of the full solid angle and consists of a helium-based multilayer drift chamber (MDC), a plastic scintillator time-of-flight system (TOF), and a CsI(Tl) electromagnetic calorimeter (EMC), which are all enclosed in a superconducting solenoidal magnet providing a 1.0 T magnetic field. The solenoid is supported by an octagonal flux-return yoke with resistive plate counter muon identification modules interleaved with steel. The charged-particle momentum resolution at 1 GeV/ c is 0.5%, and the dE/dx resolution is 6% for electrons from Bhabha scattering. The EMC measures photon energies with a resolution of 2.5% (5%) at 1 GeV in the barrel (end cap) region. The time resolution in the TOF barrel region is 68 ps, while that in the end cap region is 110 ps. The end cap TOF system was upgraded in 2015 using multi-gap resistive plate chamber technology, providing a time resolution of 60 ps [15–17].

For this analysis, we study the BESIII data collected at center-of-mass energies between 4.15 GeV and 4.30 GeV corresponding to an integrated luminosity of 10.1 fb^{-1} . In this range, the cross section $\sigma[(e^+e^- \rightarrow \gamma X(3872))]$ has been found to be the largest [18, 19]. The full list of data points used is provided in Table I and Table II.

TABLE I. Data samples with center-of-mass energies between 4.15 GeV and 4.30 GeV. Points without references are preliminary.

Center-of-Mass Energy (MeV)	Luminosity (pb^{-1})
$4157.83 \pm 0.05 \pm 0.36$ [20]	411.31 ± 2.55
4178	3194.5 ± 0.2
$4188.59 \pm 0.15 \pm 0.68$ [21]	43.09 ± 0.03 [22]
$4189.12 \pm 0.05 \pm 0.34$ [20]	526.70 ± 2.16 [20]
$4199.15 \pm 0.05 \pm 0.34$ [20]	526.60 ± 2.05 [20]
$4207.73 \pm 0.14 \pm 0.61$ [21]	54.55 ± 0.03 [22]
$4209.39 \pm 0.06 \pm 0.34$ [20]	517.10 ± 1.81 [20]
$4217.13 \pm 0.14 \pm 0.67$ [21]	54.13 ± 0.03 [22]
$4218.93 \pm 0.06 \pm 0.32$ [20]	514.60 ± 1.80 [20]
$4226.26 \pm 0.04 \pm 0.65$ [21]	44.40 ± 0.03 [22]
$4226.26 \pm 0.04 \pm 0.65$ [21]	1047.34 ± 0.14 [22]
$4235.77 \pm 0.04 \pm 0.30$ [20]	530.30 ± 2.39 [20]
$4241.66 \pm 0.12 \pm 0.73$ [21]	55.59 ± 0.04 [22]
$4243.97 \pm 0.04 \pm 0.30$ [20]	538.10 ± 2.69 [20]
$4257.97 \pm 0.04 \pm 0.66$ [21]	523.74 ± 0.10 [22]
$4257.97 \pm 0.04 \pm 0.66$ [21]	301.93 ± 0.08 [22]
$4266.81 \pm 0.04 \pm 0.32$ [20]	531.10 ± 3.13 [20]
$4277.78 \pm 0.11 \pm 0.52$ [20]	175.70 ± 0.97 [20]
$4288.43 \pm 0.06 \pm 0.34$ [20]	501.18 ± 3.11
29 energies at low luminosities	See Table II

Monte Carlo (MC) simulated data samples generated

TABLE II. Low-luminosity scan data samples with center-of-mass energies between 4.15 GeV and 4.30 GeV. The first error on each luminosity is statistical and the second is systematic.

Center-of-mass energy (MeV)	Luminosity (pb^{-1})
4150	$7.662 \pm 0.018 \pm 0.053$ [23]
4160	$7.954 \pm 0.019 \pm 0.056$ [23]
4170	$8.008 \pm 0.039 \pm 0.130$ [23]
4180	$7.309 \pm 0.018 \pm 0.051$ [23]
4190	$7.560 \pm 0.018 \pm 0.052$ [23]
4195	$7.503 \pm 0.018 \pm 0.054$ [23]
4200	$7.582 \pm 0.018 \pm 0.053$ [23]
4203	$6.815 \pm 0.017 \pm 0.048$ [23]
4206	$7.638 \pm 0.018 \pm 0.055$ [23]
4210	$7.678 \pm 0.018 \pm 0.054$ [23]
4215	$7.768 \pm 0.019 \pm 0.054$ [23]
4220	$7.935 \pm 0.019 \pm 0.055$ [23]
4225	$8.212 \pm 0.020 \pm 0.061$ [23]
4230	$8.193 \pm 0.020 \pm 0.057$ [23]
4235	$8.273 \pm 0.020 \pm 0.057$ [23]
4240	$7.830 \pm 0.019 \pm 0.054$ [23]
4243	$8.571 \pm 0.020 \pm 0.060$ [23]
4245	$8.487 \pm 0.020 \pm 0.060$ [23]
4248	$8.554 \pm 0.020 \pm 0.059$ [23]
4250	$8.596 \pm 0.020 \pm 0.060$ [23]
4255	$8.657 \pm 0.020 \pm 0.060$ [23]
4260	$8.880 \pm 0.021 \pm 0.063$ [23]
4265	$8.629 \pm 0.020 \pm 0.061$ [23]
4270	$8.548 \pm 0.020 \pm 0.060$ [23]
4275	$8.567 \pm 0.020 \pm 0.060$ [23]
4280	$8.723 \pm 0.021 \pm 0.060$ [23]
4285	$8.596 \pm 0.020 \pm 0.059$ [23]
4290	$9.010 \pm 0.021 \pm 0.062$ [23]
4300	$8.453 \pm 0.020 \pm 0.064$ [23]

with a GEANT4-based [24] software package, which includes the geometric description of the BESIII detector and the detector response, are used to determine detection efficiencies and to estimate backgrounds. The simulation models the beam energy spread and initial state radiation (ISR) in the e^+e^- annihilations with the generator KKMC [25, 26]. The inclusive MC sample includes the production of open charm processes, the ISR production of vector charmonium(-like) states, and the continuum processes incorporated in KKMC [25, 26]. All particle decays are modeled with EVTGEN [27, 28] using branching fractions either taken from the Particle Data Group (PDG) [29], when available, or otherwise estimated with LUNDCHARM [30, 31]. Final state radiation from charged final-state particles is incorporated using the PHOTOS package [32].

Signal MC samples are generated for the processes $e^+e^- \rightarrow \gamma X(3872)$ with $X(3872) \rightarrow \pi^0\pi^0\chi_{cJ}$ ($J = 0, 1, 2$) and $X(3872) \rightarrow \pi^+\pi^-J/\psi$ for the purposes of calculating the reconstruction efficiency and optimizing the event selection. The decay $e^+e^- \rightarrow \gamma X(3872)$ is taken to be dominated by an electric dipole transition with the angular distribution described as $1 - \frac{1}{3} \cos^2\theta$. The decays of the $X(3872)$ to $\pi^0\pi^0\chi_{cJ}$ are generated uni-

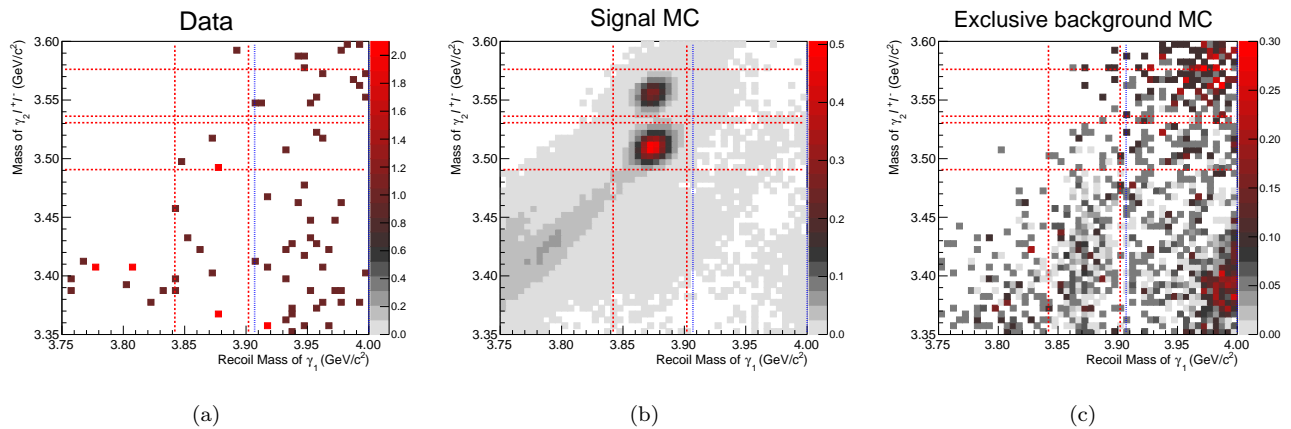


FIG. 1. Invariant mass spectrum for $\gamma_2 l^+ l^-$ versus the recoil mass of γ_1 around the signal region for data (left), signal MC (center), and exclusive background MC (right). Events are subject to all selection criteria discussed in Section III except those eliminating multiple combinations. Dashed red lines denote the $X(3872)$ signal region in the search channel and the dotted blue lines indicate the sideband region in the search channel. Due to limited phase space below the $X(3872)$ mass, only the high mass sideband is used. Though present in the MC, no χ_{c0} signal is seen. An excess of events in the lower-left of the signal MC plot is the result of incorrectly combined $\chi_{c1,2}$ candidates owing to the presence of two photons in the search channel final state.

formly according to a phase space model. The normalization channel decays $X(3872) \rightarrow \pi^+ \pi^- J/\psi$ are described with an S -wave model through the intermediate process $X(3872) \rightarrow \rho^0 J/\psi$ with $\rho \rightarrow \pi^+ \pi^-$. For visualization, all three search channel modes are generated with the same branching fraction $\mathcal{B}(X(3872) \rightarrow \pi^0 \chi_{c1})$ measured in Ref. [5]. Samples are generated with four thousand times more events than expected in the data and scaled down to reduce statistical fluctuations.

A variety of exclusive background MC samples are generated to study J/ψ peaking backgrounds. These backgrounds share final states identical to, or potentially misidentified as, the search channel, resulting in peaking backgrounds in or near the signal region. The number of events generated for each decay is computed as a product of previously measured luminosities, cross sections [29, 33–39], and branching fractions. Samples are generated with excess statistics and scaled down to the appropriate luminosity. The J/ψ decays only to $e^+ e^-$ or $\mu^+ \mu^-$, and the $\psi(3686)$ may decay to $\pi\pi J/\psi$, $\eta J/\psi$, $\pi^0 J/\psi$, $\gamma\gamma J/\psi$, or $\gamma\chi_{cJ}$. The background decays studied for this analysis are listed in Table III. All light hadrons decay inclusively.

The J/ψ sideband events are used to estimate non- J/ψ backgrounds. We choose the J/ψ sideband using $44 \text{ MeV}/c^2 \leq |M(l^+ l^-) - M(J/\psi)| \leq 176 \text{ MeV}/c^2$, where $M(l^+ l^-)$ is the measured invariant mass of the final-state leptons and $M(J/\psi)$ is the nominal J/ψ mass tabulated in the PDG [29], resulting in a sideband four times wider than the signal region.

TABLE III. Decays used to generate exclusive MC.

Group	Process
J/ψ peaking	$e^+ e^- \rightarrow \omega \chi_{cJ}$
	$e^+ e^- \rightarrow \eta J/\psi$
	$e^+ e^- \rightarrow \eta' J/\psi$
	$e^+ e^- \rightarrow \pi^+ \pi^- \psi'$
	$e^+ e^- \rightarrow \pi^0 \pi^0 \psi'$
	$e^+ e^- \rightarrow \pi^+ \pi^- J/\psi$
$X(3823)$ peaking	$e^+ e^- \rightarrow \pi^0 \pi^0 X(3823)$
	ISR $e^+ e^- \rightarrow \gamma \psi'$
$X(3872)$ peaking	$X(3872) \rightarrow \pi^+ \pi^- J/\psi$
	$X(3872) \rightarrow \pi^0 \chi_{cJ}$
	$X(3872) \rightarrow \gamma \psi'$
	$X(3872) \rightarrow \gamma J/\psi$
	$X(3872) \rightarrow \omega J/\psi$

III. EVENT SELECTION

The final states for both the normalization and search channels are fully reconstructed. For the normalization channel, we use the same event selection criteria as in the single-pion analysis [5]. Details for the selection of the search channel are described in the following.

Charged tracks detected in the MDC are required to be within a polar angle (θ) range of $|\cos\theta| < 0.93$, where θ is defined with respect to the z -axis, which is the symmetry axis of the MDC. Their distance of closest approach to the interaction point (IP) must be less than 10 cm along the z -axis, $|V_z|$, and less than 1 cm in the transverse plane, $|V_{xy}|$. To distinguish between electrons and

muons, each electron pair is required to have at least one candidate with $E/p > 0.85$, while each muon pair requires both candidates to have $E/p < 0.25$, where E is the energy of the candidate deposited in the EMC and p is the momentum of the candidate reconstructed in the MDC. To select J/ψ events, we require the l^+l^- mass to be within $33 \text{ MeV}/c^2$ of the nominal J/ψ mass.

Photons are identified as showers within the EMC. Energy deposited in nearby TOF counters is added to the shower energy. The deposited energy of each shower must be more than 25 MeV in the barrel region ($|\cos\theta| < 0.80$) and more than 50 MeV in the end cap region ($0.86 < |\cos\theta| < 0.92$). To suppress electronic noise and showers unrelated to the event, the difference between the EMC time and the event start time is required to be within $[0, 700] \text{ ns}$. The π^0 candidates are formed from pairs of photons and are required to satisfy $107 \text{ MeV}/c^2 < M(\gamma\gamma) < 163 \text{ MeV}/c^2$. In addition, a π^0 mass fit is performed separately for each pair and $\chi^2 < 2500$ is imposed.

A six constraint (6C) kinematic fit is performed on the final-state particles. Momentum and energy account for four of these constraints, while the remaining two constraints comprise π^0 mass constraints. We require $\chi_{6C}^2/\text{d.o.f} < 9.0$ for χ_{c1} events and $\chi_{6C}^2/\text{d.o.f} < 8.0$ for χ_{c2} events, where $\chi_{6C}^2/\text{d.o.f}$ is the 6C kinematic fit χ^2 statistic per degree of freedom. These values were chosen by optimizing over a figure of merit (FOM)

$$FOM = \sqrt{-2 \ln \frac{P(\mu\tau; N_{\text{bkg}})P(\mu; N_{\text{sig}})}{P(N_{\text{bkg}}; N_{\text{bkg}})P(N_{\text{sig}}; N_{\text{sig}})}}, \quad (1)$$

which is a direct computation of the expected significance where P is the Poisson distribution, N_{sig} is the number of events in the signal region, N_{bkg} is the number of events in the background region, and τ is the expected ratio of background events in the background region to background events in the signal region. The signal and background regions are described in the next section. The free parameter μ is chosen to maximize the numerator. Because N_{sig} and N_{bkg} are not integers in exclusive MC, the figure of merit is computed by sampling Poisson distributions with means N_{sig} and N_{bkg} and averaging the results.

Various vetoes are also applied to the search channel to reject the peaking backgrounds modeled by the exclusive background MC listed in Table III from the signal region. These include an $\eta^{(\prime)} \rightarrow \gamma\gamma\pi^0\pi^0$ veto to remove $e^+e^- \rightarrow \eta^{(\prime)}J/\psi$ and a $\psi(3686) \rightarrow \gamma\gamma l^+l^-$ veto to remove $e^+e^- \rightarrow \pi^0\pi^0\psi(3686)$. These vetoes are optimized by the FOM defined in Eq. 1. A list of all optimized requirements is given in Table IV.

In addition, due to the large number of photons in the final state, we address the issue of multiple-counting through two approaches. For photons originating from π^0 decays, we select the combination with the lowest $\chi^2/\text{d.o.f}$. value from the kinematic fit. The remaining

two photons, not associated with π^0 decays, are differentiated by selecting the mass combination of any photon with $\pi^0\pi^0 l^+l^-$ closest to the relevant world average χ_{cJ} mass [29].

After these selection criteria, Fig. 1 shows the invariant mass of the $\gamma_2 l^+ l^-$ system vs. the mass recoiling against γ_1 . The signal MC sample shows clear χ_{c1} and χ_{c2} signals, but no χ_{c0} due to its strongly suppressed radiative decay.

To select χ_{cJ} candidates, we require $M(\gamma_2 l^+ l^-) - M(l^+ l^-) + M(J/\psi)$ to be within 20 MeV of the nominal χ_{cJ} mass for a particular J . The invariant mass spectra of the $l^+ l^-$ and $\gamma_2 l^+ l^-$ systems, along with their corresponding requirements, are shown in Fig. 2.

TABLE IV. Processes we choose to veto and their optimized selection criteria.

Cut	Value
Kinematic fit ($J = 1$)	$\chi^2/\text{d.o.f} < 9.0$
Kinematic fit ($J = 2$)	$\chi^2/\text{d.o.f} < 8.0$
$e^+e^- \rightarrow \eta J/\psi$ veto	$ M(\gamma_1\gamma_2\pi^0\pi^0) - M(\eta) > 40 \text{ MeV}/c^2$
$e^+e^- \rightarrow \eta' J/\psi$ veto	$ M(\gamma_1\gamma_2\pi^0\pi^0) - M(\eta') > 15 \text{ MeV}/c^2$
$e^+e^- \rightarrow \pi^0\pi^0\psi'$ veto	$ M(\gamma_1\gamma_2 l^+ l^-) - M(\psi') > 30 \text{ MeV}/c^2$

IV. SIGNAL YIELDS

Due to the low number of events in the search channel, signal yields are determined using a counting method. We measure the number of events N_{sig} in the signal region, defined as the region in the recoil mass spectrum of γ_1 against the CM within 30 MeV of the nominal $X(3872)$ mass, and the number of events N_{bkg} in the background region, defined as the region 35 MeV above the nominal $X(3872)$ mass in the recoil mass spectrum of γ_1 against the CM and extending to the end of the plot window at 4.0 GeV . Phase space is limited at masses below the $X(3872)$ peak, so this region is not considered to estimate the background. There is good agreement between the number of data events in the $X(3872)$ sidebands and the number of events predicted by the J/ψ sidebands and exclusive background MC in those same $X(3872)$ sidebands. As such, we estimate the background in the signal region by assuming the ratio τ of background events in the signal region to the number of background events in the sideband region is the same as the ratio calculated from MC. The signal yield in the search channel is therefore $N_{\text{search}} = N_{\text{sig}} - \tau N_{\text{bkg}}$. Asymmetric 1σ uncertainties on the yield are calculated using N_{sig} , N_{bkg} , and τ as inputs for the Rolke method [40]. Data and MC measured in each region of the search channel are plotted in Fig. 3.

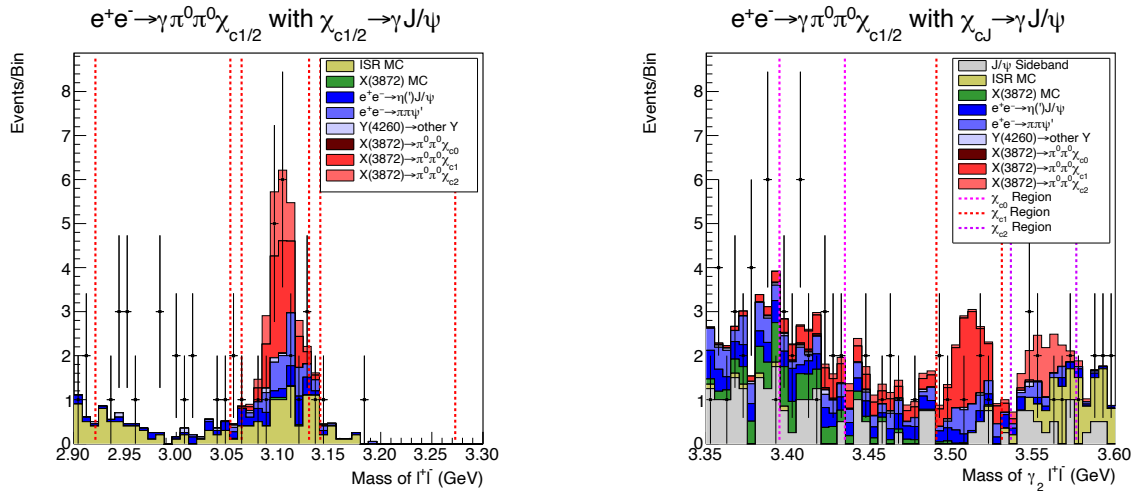


FIG. 2. Masses of J/ψ (left) and χ_{cJ} (right) candidates. The stacked histograms give the MC and, on the right, the J/ψ data sidebands. The histogram labeled “other Y” contains all J/ψ -peaking background MC not specifically plotted with its own style. The points with error bars are the data. On the left, the center lines denote the J/ψ signal region in the search channel and the outer lines denote the boundaries of the J/ψ data sidebands. On the right, the leftmost pair of lines indicates the boundaries of the χ_{c0} signal region, which we are not sensitive to, while the center and right pairs show the χ_{c1} and χ_{c2} signal selections, respectively. All cuts are included except those on the variable along the horizontal axis and the minimum $\chi^2/\text{d.o.f.}$ selection. For the right plot, the $\chi^2/\text{d.o.f.}$ requirement for χ_{c1} events is used for all χ_{cJ} candidate masses.

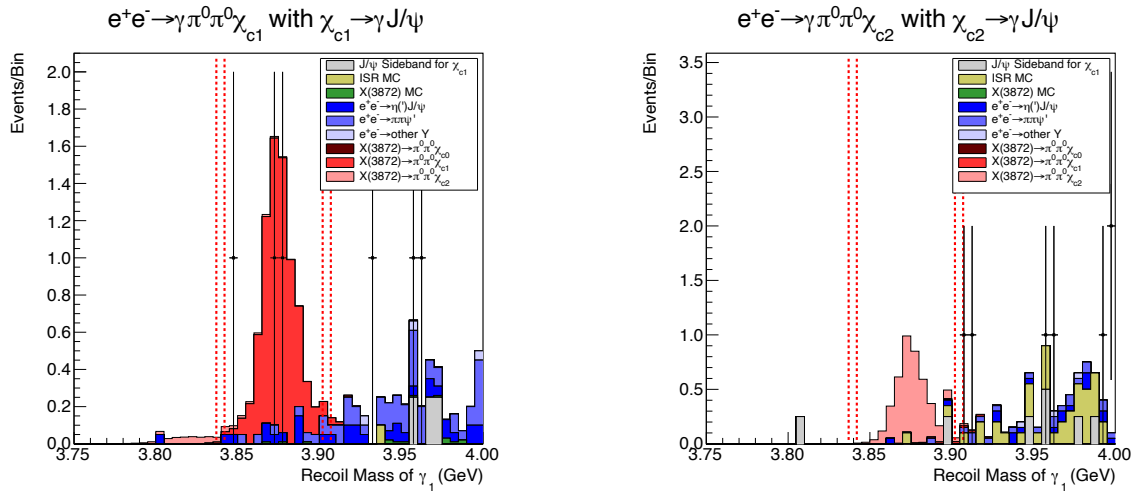


FIG. 3. Masses of $X(3872)$ candidates in the χ_{c1} and χ_{c2} regions. The data is given by points, while the stacked histograms represent exclusive background MC and J/ψ data sidebands. The histogram labeled “other Y” contains all J/ψ -peaking background MC not specifically plotted with its own style. The inner dashed lines give the signal region and the outer dashed lines give the background regions. A counting method is used to determine the number of $X(3872)$ events in the signal region.

For consistency, this counting method is also used to compute the signal yield in the normalization channel. Here we use the signal and background regions defined in the $X(3872) \rightarrow \pi^0 \chi_{cJ}$ analysis [5]: the signal region is defined as the region within 15 MeV of the $X(3872)$ mass in the recoil mass spectrum of γ_1 against the CM, and the background region is defined between 25 MeV and 85 MeV from the $X(3872)$ mass on both sides in the recoil mass spectrum of γ_1 against the CM. As for the

search channel, the Rolke method is used to compute the uncertainties on the yield. Data measured in the signal and background regions of the normalization channel are plotted in Fig. 4.

The measured numbers of events, as well as background ratios, efficiencies, and the resulting signal yields, are listed in Table V for all modes. These values are used

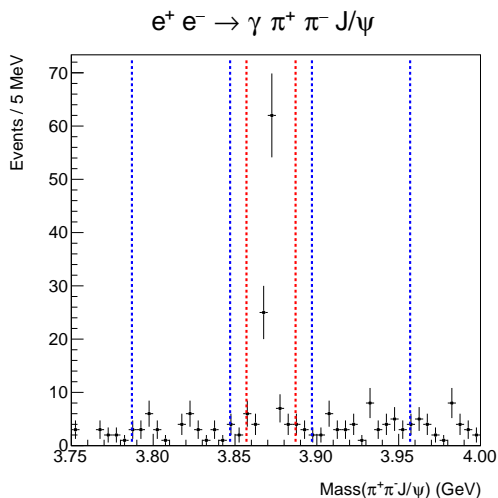


FIG. 4. Mass of $X(3872)$ candidates in the normalization channel. The signal region is denoted by red lines and the sideband region by blue lines. A counting method is used to determine the number of $X(3872)$ events in the signal peak.

to compute the ratio $R_{\chi_{cJ}}$, given as

$$\begin{aligned}
 R_{\chi_{cJ}} &= \frac{\mathcal{B}(X(3872) \rightarrow \pi^0 \pi^0 \chi_{cJ})}{\mathcal{B}(X(3872) \rightarrow \pi^+ \pi^- J/\psi)} \\
 &= \frac{N_{\text{search}} \epsilon_{\text{norm}}}{N_{\text{norm}} \epsilon_{\text{search}} \mathcal{B}(\pi^0 \rightarrow \gamma\gamma)^2 \mathcal{B}(\chi_{cJ} \rightarrow \gamma J/\psi)}, \quad (2)
 \end{aligned}$$

where N_{search} and N_{norm} are the measured number of signal events in the search and normalization channels, respectively, and ϵ_{search} and ϵ_{norm} are the efficiencies calculated for the search and normalization channels, respectively. The branching fractions $\mathcal{B}(\pi^0 \rightarrow \gamma\gamma)$ and $\mathcal{B}(\chi_{cJ} \rightarrow \gamma J/\psi)$ are those tabulated by the PDG [29].

TABLE V. Summary of signal yields, efficiencies, and other values used in the calculation of the branching fraction ratios $\frac{\mathcal{B}(X(3872) \rightarrow \pi^0 \pi^0 \chi_{c1,2})}{\mathcal{B}(X(3872) \rightarrow \pi^+ \pi^- J/\psi)}$.

Mode	N_{sig}	N_{bkg}	ϵ	τ	$N_{\text{search/norm}}$
$X(3872) \rightarrow \pi^0 \pi^0 \chi_{c1}$	3.0	3.0	7.9%	0.184	2.4 $^{+1.8}_{-1.9}$
$X(3872) \rightarrow \pi^0 \pi^0 \chi_{c2}$	0.0	6.0	8.1%	0.091	0.0 $^{+1.4}_{-0.0}$
$X(3872) \rightarrow \pi^+ \pi^- J/\psi$	107.0	80.0	33.9%	0.250	87.0 $^{+10.9}_{-10.3}$

V. SYSTEMATIC UNCERTAINTIES

A variety of sources of systematic uncertainties on the branching fraction ratio are addressed. In addition to quantities such as the cross-section and luminosity, several uncertainties on the branching fraction

$\mathcal{B}(X(3872) \rightarrow \pi^0 \pi^0 \chi_{c1,2})$ cancel upon computing the ratio. Here we describe these remaining systematic uncertainties on the ratio $R_{\chi_{cJ}}$, given by Eq. 2.

A. Photon detection and charged track efficiencies

Photons and charged tracks in the BESIII detector were previously measured to have systematic uncertainties of 1% per photon [41] and charged track [42]. In the ratio, five photons (four from π^0 decays and one from the χ_{cJ} decay) and two charged pions are uncanceled. Therefore, the photon detection efficiency systematic uncertainty is 5% and the charged track reconstruction efficiency is 2%.

B. Input branching fractions

The remaining branching fractions $\mathcal{B}(\pi^0 \rightarrow \gamma\gamma)$ and $\mathcal{B}(\chi_{cJ} \rightarrow \gamma J/\psi)$ do not cancel in the branching fraction ratio. These branching fractions and their uncertainties are taken directly from the PDG [29].

C. Kinematic fit

The systematic uncertainty due to the kinematic fit is addressed by comparing the effect of a loosened $\chi^2/\text{d.o.f.}$ cut to the nominal value on control samples. The process $e^+e^- \rightarrow \eta J/\psi$ with $\eta \rightarrow \gamma\gamma\pi^0\pi^0$ is used to estimate contributions to the uncertainty from the search channel, while the process $e^+e^- \rightarrow \gamma_{\text{ISR}}\psi'$, with $\psi(3686) \rightarrow \pi^+\pi^- J/\psi$, is used to estimate contributions from the normalization channel. The efficiency of the $\chi^2/\text{d.o.f.}$ selection is computed in signal MC for the search and normalization channels by dividing the number of events with the nominal $\chi^2/\text{d.o.f.}$ by the number of events with a loose selection of $\chi^2/\text{d.o.f.} < 25.0$. The same efficiency is then calculated in data for both channels. The ratio between the search and normalization channels is then computed in MC and in data. The difference between the values of these ratios, 1.7% for χ_{c1} and 2.1% for χ_{c2} , is taken as the systematic uncertainty.

D. E/p cut

The systematic uncertainty on the E/p cut is computed in the same way as the kinematic fitting systematic uncertainty in Section V C. The nominal selection criteria in the search and normalization control samples are relaxed to $E/p < 0.5$ for both muons and $E/p > 0.5$ for either electron. Ratios of efficiencies between the search

and normalization channels are calculated in MC and data and the difference between these ratios, 2.7% for χ_{c1} and 2.4% for χ_{c2} , is taken as the systematic uncertainty in the E/p selection.

E. Decay model

Generating signal MC events containing an $X(3872)$ requires an assumption about the decay model used to describe the production mechanism $e^+e^- \rightarrow \gamma X(3872)$. This results in a systematic uncertainty that we estimate by generating $e^+e^- \rightarrow \gamma X(3872)$ signal MC with four alternative decay models. The nominal model is based on the model for the decay $\psi(3686) \rightarrow \gamma\chi_{c1}$; the process is assumed to be E1 dominant where the photon has the angular distribution $1 - \frac{1}{3}\cos^2\theta$ [43]. The four variations are: (1) phase space; (2) $L = 0, S = 1$; (3) $L = 2, S = 1$; and (4) $L = 2, S = 2$. Here, S is the combined spin of the γ and the $X(3872)$ and L is the orbital angular momentum between them.

We further introduce two systematic variations on the decay model for $X(3872) \rightarrow \rho^0 J/\psi$ used for the normalization channel. These are (1) $L = 2, S = 1$ and (2) $L = 2, S = 2$, where S is the combined spin of the ρ^0 and J/ψ and L is the orbital angular momentum between them. These two configurations, alongside the nominal S -wave, are the only partial waves allowed for $X(3872) \rightarrow \rho^0 J/\psi$ by angular momentum conservation.

The greatest difference between efficiency ratios computed with the nominal model and one of the model variations, 11.0% for χ_{c1} and 9.2% for χ_{c2} , is taken to be the systematic uncertainty.

F. Efficiency ratio energy dependence

In order for the cross section and luminosity to cancel in the ratio given in Eq. 2, we assume the reconstruction efficiency at each CM energy used in the calculation is identical. In practice, this assumption is not exactly true, resulting in an additional systematic uncertainty caused by some energy dependence on the efficiency ratio. To assess this uncertainty, the weighted average of the efficiency ratio over the center-of-mass-energy range is calculated, with the weight of each energy point given by the value of the nominal $\sigma(e^+e^- \rightarrow \gamma X(3872))$ lineshape. The resulting average is taken as the nominal value. The mass and width parameters of this lineshape are then varied by one sigma in either direction in every possible combination and an average efficiency ratio is calculated for each. The greatest deviation from the nominal value, 0.4% for χ_{c1} and 0.5% for χ_{c2} , is taken to be the systematic uncertainty.

G. Total systematic uncertainties

All systematic uncertainties for a particular mode are summed in quadrature to give the total systematic uncertainty, summarized in Table VI.

TABLE VI. Relative systematic uncertainties, given in percent.

Source	χ_{c1} (%)	χ_{c2} (%)
Photon selection	5.0	5.0
Tracking	2.0	2.0
Input branching fractions	2.9	2.6
Kinematic fit	1.7	2.1
E/p	2.7	2.4
Decay model	11.0	9.2
Energy dependence	0.4	0.5
Total	13.0	11.4

VI. UPPER LIMIT CALCULATIONS

Due to the low significance of the signal yields for both the χ_{c1} and χ_{c2} modes, we calculate upper limits on the number of signal events in the search channel using the Rolke method [40], at the 90% confidence level. In addition, the total systematic uncertainties given in Table VI, added in quadrature with the maximum uncertainty on the normalization channel yield, are treated as an uncertainty on the efficiency. These upper limits are then divided by the normalization channel measurement to obtain the upper limit on the ratio. The resulting upper limits on the branching fraction ratios are

$$\frac{\mathcal{B}(X(3872) \rightarrow \pi^0\pi^0\chi_{c1})}{\mathcal{B}(X(3872) \rightarrow \pi^+\pi^-J/\psi)} < 1.1 \quad (3)$$

and

$$\frac{\mathcal{B}(X(3872) \rightarrow \pi^0\pi^0\chi_{c2})}{\mathcal{B}(X(3872) \rightarrow \pi^+\pi^-J/\psi)} < 0.5. \quad (4)$$

These upper limits on the branching fraction ratios serve to further disfavor the conventional charmonium hypothesis for the $X(3872)$ and are consistent with compact tetraquark and hadronic molecule predictions.

VII. SUMMARY

Our search for the decays $X(3872) \rightarrow \pi^0\pi^0\chi_{c1,2}$ in BESIII data between 4.15 GeV and 4.30 GeV did not yield any evidence for these processes. The upper limits of $R_{\chi_{cJ}}$ at the 90% confidence level were determined

for both channels, with $\frac{\mathcal{B}(X(3872) \rightarrow \pi^0 \pi^0 \chi_{c1})}{\mathcal{B}(X(3872) \rightarrow \pi^+ \pi^- J/\psi)} < 1.1$ and $\frac{\mathcal{B}(X(3872) \rightarrow \pi^0 \pi^0 \chi_{c2})}{\mathcal{B}(X(3872) \rightarrow \pi^+ \pi^- J/\psi)} < 0.5$. The χ_{c1} result clearly disfavors a conventional charmonium interpretation of the $X(3872)$, which is expected to exhibit a branching fraction ratio of $\frac{\mathcal{B}(X(3872) \rightarrow \pi^0 \pi^0 \chi_{c1})}{\mathcal{B}(X(3872) \rightarrow \pi^+ \pi^- J/\psi)} \approx 12.5$ [9]. In addition, both results are consistent with models describing $X(3872)$ as a four-quark state [10], although the statistics at the moment is insufficient to validate these predictions.

ACKNOWLEDGMENTS

The BESIII Collaboration thanks the staff of BEPCII and the IHEP computing center for their strong support. This work is supported in part by National Key R&D Program of China under Contracts Nos. 2020YFA0406300, 2020YFA0406400, 2023YFA1606000; National Natural Science Foundation of China (NSFC) under Contracts Nos. 11635010, 11735014, 11835012, 11935015, 11935016, 11935018, 11961141012, 12025502, 12035009, 12035013, 12061131003, 12192260, 12192261, 12192262, 12192263, 12192264, 12192265, 12221005, 12225509, 12235017; the Chinese Academy of Sciences (CAS) Large-Scale Scientific Facility Program; the CAS

Center for Excellence in Particle Physics (CCEPP); Joint Large-Scale Scientific Facility Funds of the NSFC and CAS under Contract No. U1832207; CAS Key Research Program of Frontier Sciences under Contracts Nos. QYZDJ-SSW-SLH003, QYZDJ-SSW-SLH040; 100 Talents Program of CAS; The Institute of Nuclear and Particle Physics (INPAC) and Shanghai Key Laboratory for Particle Physics and Cosmology; European Union's Horizon 2020 research and innovation programme under Marie Skłodowska-Curie grant agreement under Contract No. 894790; German Research Foundation DFG under Contracts Nos. 455635585, Collaborative Research Center CRC 1044, FOR5327, GRK 2149; Istituto Nazionale di Fisica Nucleare, Italy; Ministry of Development of Turkey under Contract No. DPT2006K-120470; National Research Foundation of Korea under Contract No. NRF-2022R1A2C1092335; National Science and Technology fund of Mongolia; National Science Research and Innovation Fund (NSRF) via the Program Management Unit for Human Resources & Institutional Development, Research and Innovation of Thailand under Contract No. B16F640076; Polish National Science Centre under Contract No. 2019/35/O/ST2/02907; The Swedish Research Council; U. S. Department of Energy under Contract No. DE-FG02-05ER41374.

-
- [1] S. K. Choi *et al.* (Belle Collaboration), *Phys. Rev. Lett.* **91**, 262001 (2003).
- [2] T. Barnes and S. Godfrey, *Phys. Rev. D* **69**, 054008 (2004).
- [3] R. Aaij *et al.* (LHCb Collaboration), *Phys. Rev. D* **102**, 092005 (2020).
- [4] R. Aaij *et al.* (LHCb Collaboration), *Journal of High Energy Physics* **2020**, 1 (2020).
- [5] M. Ablikim *et al.* (BESIII Collaboration), *Phys. Rev. Lett.* **122**, 202001 (2019).
- [6] N. A. Törnqvist, *Phys. Lett. B* **590**, 209 (2004).
- [7] L. Maiani, F. Piccinini, A. D. Polosa, and V. Riquer, *Phys. Rev. D* **71**, 014028 (2005).
- [8] Y. Dong, A. Faessler, T. Gutsche, and V. E. Lyubovitskij, *Phys. Rev. D* **77**, 094013 (2008).
- [9] S. Dubynskiy and M. B. Voloshin, *Phys. Rev. D* **77**, 014013 (2008).
- [10] S. Fleming and T. Mehen, *Phys. Rev. D* **78**, 094019 (2008).
- [11] M. Ablikim *et al.* (BESIII Collaboration), *Phys. Rev. D* **105**, 072009 (2022).
- [12] M. Ablikim *et al.* (BESIII Collaboration), *Nucl. Instrum. Meth. A* **614**, 345 (2010).
- [13] C. Yu *et al.*, in *7th International Particle Accelerator Conference* (2016) p. TUYA01.
- [14] M. Ablikim *et al.* (BESIII Collaboration), *Chin. Phys. C* **44**, 040001 (2020).
- [15] X. Li, Y. Sun, C. Li, *et al.*, *Radiation Detection Technology and Methods* **1**, 13 (2017).
- [16] Y. X. Guo, S. S. Sun, F. F. An, *et al.*, *Radiation Detection Technology and Methods* **1**, 15 (2017).
- [17] P. Cao, H. Chen, M. Chen, *et al.*, *Nucl. Instrum. Meth. A* **953**, 163053 (2020).
- [18] M. Ablikim *et al.* (BESIII Collaboration), *Phys. Rev. Lett.* **112**, 092001 (2014).
- [19] M. Ablikim *et al.* (BESIII Collaboration), *Phys. Rev. Lett.* **122**, 232002 (2019).
- [20] M. Ablikim *et al.* (BESIII Collaboration), *Chin. Phys. C* **45**, 103001 (2021).
- [21] M. Ablikim *et al.* (BESIII Collaboration), *Chin. Phys. C* **40**, 063001 (2016).
- [22] M. Ablikim *et al.* (BESIII Collaboration), *Chin. Phys. C* **39**, 093001 (2015).
- [23] M. Ablikim *et al.* (BESIII Collaboration), *Chin. Phys. C* **41**, 063001 (2017).
- [24] S. Agostinelli *et al.*, *Nucl. Instrum. Meth. A* **506**, 250 (2003).
- [25] S. Jadach, B. F. L. Ward, and Z. Wąs, *Phys. Rev. D* **63**, 113009 (2001).
- [26] S. Jadach, B. F. L. Ward, and Z. Wąs, *Computer Physics Communications* **130**, 260 (2000).
- [27] D. J. Lange, *Nucl. Instrum. Meth. A* **462**, 152 (2001).
- [28] R. G. Ping, *Chin. Phys. C* **32**, 599 (2008).
- [29] R. L. Workman *et al.* (Particle Data Group), *PTEP* **2022**, 083C01 (2022).
- [30] J. C. Chen, G. S. Huang, X. R. Qi, D. H. Zhang, and Y. S. Zhu, *Phys. Rev. D* **62**, 034003 (2000).
- [31] R. L. Yang, R. G. Ping, and H. Chen, *Chin. Phys. Lett.* **31**, 061301 (2014).

- [32] E. Richter-Was, Phys. Lett. B **303**, 163 (1993).
- [33] M. Ablikim *et al.* (BESIII Collaboration), Phys. Rev. Lett. **122**, 232002 (2019).
- [34] M. Ablikim *et al.* (BESIII Collaboration), Phys. Rev. D **103**, L091102 (2021).
- [35] M. Ablikim *et al.* (BESIII Collaboration), Phys. Rev. D **99**, 091103 (2019).
- [36] M. Ablikim *et al.* (BESIII Collaboration), Phys. Rev. D **93**, 011102 (2016).
- [37] M. Ablikim *et al.* (BESIII Collaboration), Phys. Rev. D **96**, 032004 (2017).
- [38] M. Ablikim *et al.* (BESIII Collaboration), Phys. Rev. D **102**, 031101 (2020).
- [39] M. Ablikim *et al.* (BESIII Collaboration), Phys. Rev. D **101**, 012008 (2020).
- [40] W. A. Rolke, A. M. Lopez, and J. Conrad, Nucl. Instrum. Meth. A **551**, 493 (2005).
- [41] M. Ablikim *et al.* (BESIII Collaboration), Phys. Rev. D **81**, 052005 (2010).
- [42] M. Ablikim *et al.* (BESIII Collaboration), Phys. Rev. D **94**, 032009 (2016).
- [43] R. G. Ping and C. Y. Pang, *Monte Carlo Generators for Tau-Charm-Physics at BESIII*, Tech. Rep. (2006).